INTERNATIONAL JOURNAL FOR NUMERICAL METHODS IN FLUIDS, VOL. 5, 763–783 (1985)

A NEW METHOD FOR COMPUTING SOLENOIDAL VECTOR FIELDS ON ARBITRARY REGIONS

K. GUSTAFSON AND K. HALASI

Department of Mathematics, University of Colorado, Boulder, Colorado 80309, U.S.A.

AND

D. P. YOUNG

Boeing Computer Services, Tukwila, Washington 98188, U.S.A.

SUMMARY

We develop a new method for the efficient calculation of solenoidal vector fields on general regions. The method takes advantage of fast direct methods and uses boundary integral equations to satisfy boundary conditions. For the latter we give an effective scheme for computing far-field boundary influences (based on discrete charges). Examples and numerical results are given. The method is applicable to incompressible Navier–Stokes calculations.

KEY WORDS Solenoidal Vector Fields Fast Poisson Solvers Boundary Integral Methods Far Field Approximations Navier—Stokes Equations Capacitance Matrices

1. INTRODUCTION

The origins of this work are in a general scheme given by Gustafson[1] for determining the stability of perturbed flows by estimating the asymptotic distribution of eigenvalues of fluid dynamics operators of the form

$$-P_{\mathrm{H}}\mathbf{D}\mathbf{u} = \lambda \mathbf{u}. \tag{1}$$

Here $\mathbf{D}$ is a differential expression, e.g.

$$\mathbf{D} = \begin{bmatrix} \Delta - 1/R^2 & 0 & 0 \\ 0 & \Delta - 1/R^2 & 0 \\ 0 & 0 & \Delta \end{bmatrix} \tag{2}$$

for the three dimensional Taylor problem of flow between rotating cylinders, and P_{H} is the Helmholtz projector onto the solenoidal subspace of divergence-free vector fields, e.g.

$$P_{\mathrm{H}}\mathbf{v}(\mathrm{P}) = \mathrm{curl} \int_{\Omega} \frac{\mathrm{curl}\, \mathbf{v}(\mathrm{Q})}{4\pi R_{\mathrm{PQ}}} \tag{3}$$

for sufficiently smooth vector fields vanishing near the boundary of the domain Ω in question.

0271–2091/85/090763–21$02.10

Received 26 April 1984
Revised 27 December 1984

$A = P_H \mathbf{D}$ is a self-adjoint operator in the subspace of solenoidal vector fields and, if

$$\sum_{n=1}^{\infty} (\lambda_{n+1} - \lambda_n)^{-2} < \infty, \tag{4}$$

one may conclude that a linearized non-self-adjoint operator $A + \lambda B(\mathbf{v}_0)$ has good properties, e.g. it is spectral with real simple eigenvalues, and that the perturbed basic flow $\mathbf{v}_0$ of the full non-linear problem is stable.

As a first step in the investigation of this scheme, the direct calculation of the Helmholtz projector P_H of (3) was studied.[2] Although good convergence properties ($O(h^2)$) were achieved, the CPU times were prohibitively large for general application.

Other important applications require numerical solenoidal projection. Reference 2 gives a partial survey of methods that are used to deal with the solenoidal condition. A more recent survey, especially for finite element methods, is given by Fix.[3] Further information for the finite element approach can be obtained from the papers of Gresho, Lee and Sani,[4] Sani *et al.*,[5] Fortin[6] and Gustafson and Hartman.[7] Considerable work continues on this problem.

In our opinion, the most efficient approach is to decompose, by means of fast Poisson solvers, $(L^2(\Omega))^n$ as the sum of three subspaces

$$(L^2(\Omega))^n = H_1 \oplus H_2 \oplus H_3, \tag{5}$$

where H_1 is the potential component of the vector field (both divergence-free and curl-free), H_2 is the strictly solenoidal component (divergence-free, not curl-free) and H_3 is the irrotational component (curl-free, not divergence-free). The projection algorithm we propose is the following.

Algorithm

Given an arbitrary n-component vector field $\mathbf{v}$ in $(L^2(\Omega))^n$ over a general n-dimensional region Ω:

1. Solve the Poisson–Dirichlet problem

$$\begin{aligned} \nabla^2 \phi_3 &= \operatorname{div} \mathbf{v}, \quad \text{in } \Omega, \\ \phi_3 &= 0, \qquad \text{on } \partial\Omega; \end{aligned} \tag{6}$$

   let $\mathbf{v}_3 = \nabla \phi_3$.

2. Solve the Poisson–Neumann problem

$$\begin{aligned} \nabla^2 \phi_1 &= 0, \qquad \text{in } \Omega, \\ \frac{\partial \phi_1}{\partial n} &= \mathbf{n} \cdot \mathbf{v} - \frac{\partial \phi_3}{\partial n}, \quad \text{on } \partial\Omega; \end{aligned} \tag{7}$$

   let $\mathbf{v}_1 = \nabla \phi_1$.

3. Let $\mathbf{v}_2 = \mathbf{v} - \mathbf{v}_3 - \mathbf{v}_1$. (8)

Note that $\mathbf{n} \cdot \mathbf{v}_2 = 0$ on $\partial\Omega$. This is the impermeable boundary condition and thus H_2 is the subspace of vector fields weakly solenoidal not only in Ω but also on $\partial\Omega$. If one wishes to obtain $\mathbf{v}_2$ with just one Poisson solve one should solve the inhomogeneous Poisson–Neumann problem

$$\begin{aligned} \nabla^2 \phi &= \operatorname{div} \mathbf{v}, \quad \text{in } \Omega, \\ \frac{\partial \phi}{\partial n} &= \mathbf{n} \cdot \mathbf{v}, \qquad \text{on } \partial\Omega, \end{aligned} \tag{9}$$

and let $\mathbf{v}_2 = \mathbf{v} - \nabla \phi$.

We remark that for more general boundary conditions (e.g. mixed, Robin), variations of this decomposition of an arbitrary vector field into Poisson problems may be derived.

The method given here uses fast direct solvers to compute the domain contribution ϕ_3 (step 1 in the above algorithm) and boundary integral equations to compute the boundary contributions (step 2 of the algorithm). Boundary integral methods have been used for many years in engineering calculations for problems where resolution of complex boundaries is important.[8–10] Their use in conjunction with fast direct methods has been suggested by Mayo[11] and Johnson and James.[12] When applied in the setting of panel methods, they have been particularly successful for the calculation of linear potential flow about complex configurations. A similar setting is found in the context of capacitance matrices.[13–15]

The method presented here has the advantage that by use of panels, complicated boundaries are represented more faithfully than with standard finite differences. The resulting boundary integral equations have the normal derivative of the fundamental singularity as kernel and hence as is well known from potential theory are Fredholm operators. For this potential theory see for example Reference 16. Some of the relevant results are summarized by Proskurowski and Widlund[15] and some of the numerical considerations may be found in Reference 17. A consistent discretization $I + K_h$, h denoting panel length, constructed so as to converge uniformly to $I + K$ as $h \to 0$, will have its eigenvalues converging to those of $I + K$. This follows essentially from the upper semicontinuity of the spectrum, and more specifically, from the continuity of a finite system of eigenvalues under small perturbation. Thus, for h sufficiently small, the condition numbers of the corresponding linear systems are bounded independent of the number of boundary elements. See References 18 and 19 for comparable results for finite difference capacitance matrices and finite elements, respectively.

On the other hand, for the domain contribution from (6), we may use any fast Poisson solver, in particular methods based on finite differences combined with convolutions. The method may therefore be regarded as a hybrid.

We have not succeeded in the eigenvalue calculation for the Taylor flow problem mentioned at the beginning. We know of only one such calculation that has been carried out in another context, that of structures, by Krumhaar,[20] which required simplifications of the model and assumptions of symmetry to reduce the problem to a system of ordinary differential equations. Similar simplifying assumptions to obtain ordinary differential equations for the Taylor problem by Richtmyer[21] allowed some calculations but failed to determine stability in the sense of a strange attractor.

We are led to the view that to approach general three dimensional flow problems on general regions great attention to efficiency and effectiveness will be needed, with considerable preliminary numerical experimentation. The present paper may be regarded as a contribution in that direction. In Section 2 we describe the hybrid method. We restrict attention to general regions Ω in two dimensions and to piecewise linear (panel) approximations to $\partial\Omega$ for the boundary contributions, which are obtained by collocation. The domain contributions are obtained by embedding Ω in larger rectangles and then using fast direct methods. In Section 3 we focus attention on the calculation of the resulting near-field–far-field integrals. In aeronautics these are called the aerodynamic influence coefficients, the $\alpha_{i,j}$ corresponding to dipole charges placed near the boundary, and the $\beta_{i,j}$ corresponding to source charges placed there. In Section 4 we consider the advantages of symmetric domains and a question of source versus dipole placement. Comparisons to capacitance matrix methods and certain aspects of the resulting linear systems are also given. Some numerical results are given in Section 5. Among them are calculations on triangles, L-shaped domains and n-gons. It would be useful to examine general exterior aerofoil domains, but lack of resources did not permit the development of such general software. A number of questions

that arise are discussed in both Sections 4 and 5. Applications of the scheme to general Navier–Stokes equations in primitive variable form, and some resulting issues concerned with operator factorization near the boundary are given in Section 6.

A main novelty of our method is that point charges need not be positioned on panels when dealing with far-field calculations. A fundamental problem underlying a number of these questions, one could say it is the price one must pay to gain the efficiencies of this hybrid method, is how to cope with the interaction between and placement of boundary panels, charges, and domain finite difference grids. We have not completely resolved this problem, but we have tried in this paper to identify the key concepts, issues and questions that arise.

2. THE HYBRID METHOD

In view of Steps 1 and 2 of the algorithm of the preceding discussion, consider the general problem

$$\begin{aligned} \nabla^2\phi &= f, \quad \text{in } \Omega, \\ \alpha\phi + \beta\frac{\partial\phi}{\partial n} &= g, \quad \text{on } \partial\Omega, \end{aligned} \tag{10}$$

where Ω is a general two dimensional region with not necessarily smooth boundary (see Figure 1). The basics of the method lie in the simulation of Green's third identity

$$c(\mathrm{P})\phi(\mathrm{P}) = \int_{\partial\Omega} \frac{\partial\phi}{\partial n}\log\frac{1}{R_{\mathrm{PQ}}} - \int_{\partial\Omega}\phi\frac{\partial}{\partial n_{\mathrm{Q}}}\log\frac{1}{R_{\mathrm{PQ}}} + \iint_{\Omega} f\log\frac{1}{R_{\mathrm{PQ}}}, \tag{11}$$

where $c(\mathrm{P}) = 0$, if P is in the complement of the closure of the domain, and 2π if $P\in\Omega$. For $P\in\partial\Omega$, $c(\mathrm{P})$ is the angle formed by the tangents to the boundary at P. The vector n_{Q} denotes the outward normal to $\partial\Omega$ at Q. We use the usual notation R_{PQ} for either the vector $\overrightarrow{\mathrm{PQ}}$ or for the Euclidean distance $|\overrightarrow{\mathrm{PQ}}|$ whenever the context is clear.

Evaluating ϕ may be viewed as a potential problem in electrostatics, except that the influence function is now $\log 1/R$. There is first the domain contribution ϕ_3 due to the presence of volume charges of density f. Secondly, there is the boundary contribution ϕ_1 due to the presence on the boundary of sources and dipoles of strengths $\partial\phi_1/\partial n$ and ϕ_1, respectively. Note that our notation here is consistent with that of Section 1. The domain potential ϕ_3 is obtained directly by convolution routines for rectangular domains, whereas the boundary potential ϕ_1 is obtained from boundary integral techniques.

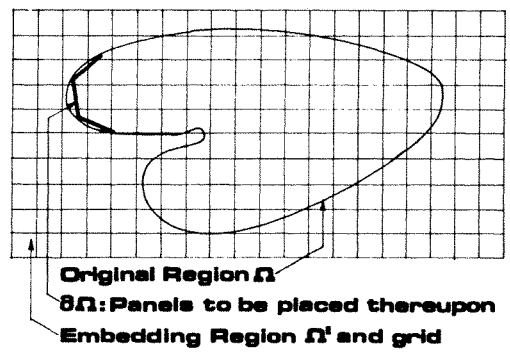

Figure 1. Region, grid and panels

The solution to (10) proceeds as follows. First we solve Step 1 of the algorithm

$$\nabla^2\phi_3 = f_e, \quad \text{in } \Omega', \tag{12}$$

where Ω' is any rectangular region containing Ω and f_e is a chosen smooth extension of f to Ω'. For (12) we employ FFT routines to compute the convolution $\phi_3 = f_e * S$ where $S = (1/2\pi)\log 1/R$. Alternatively, we may solve a discrete version of (12) on Ω by fast direct methods such as FACR(l).[22] A disadvantage to solving the convolution form of (12) is that it requires doubling the domain. We note that although Widlund *et al.*[13-15] use a periodic discrete Green's function to compute the domain contribution, we chose not to in order to retain greater flexibility in simulating boundary integral contributions. In principle in this method one has a general freedom of choice of panel and charge placement. In practice, we always chose charges as close to the panel centres as possible for optimality of error reduction.

The second step of the algorithm is to solve

$$\begin{aligned} \nabla^2\phi_1 &= 0, && \text{in } \Omega, \\ \alpha\phi_1 + \beta\frac{\partial\phi_1}{\partial n} &= g - \alpha\phi_3 - \beta\frac{\partial\phi_3}{\partial n}, && \text{on } \partial\Omega, \end{aligned} \tag{13}$$

for the 'boundary corrector' ϕ_1. In order to carry out this solution, we must approximate ϕ_3 and $\partial\phi_3/\partial n$ at the collocation points on the boundary. These points are located at the panel endpoints and the approximation is done with a second order accurate interpolation formula. Then ϕ_1 is found by a boundary integral method described immediately below. Because of the stability of the problem (13) and the fact that the boundary integral method is second order, the solution ϕ_1 will be second order accurate. Clearly $\phi_1 + \phi_3$ then solves the original problem (10).

For the description of the boundary integral method we follow for convenience and simplicity that given in a previous announcement,[23] which in turn for consistency uses the notation of Fairweather *et al.*[24] Other boundary integral formulations could be used here as well.

From the Green's identity, equation (11) with $f = 0$, we construct piecewise linear (or piecewise quadratic for higher order approximations) basis functions for $\partial\phi/\partial n$ and ϕ. Using collocation on the integral equation and its normal derivative will enforce the boundary conditions and yield a linear system for the surface singularity values. To achieve this end we partition $\partial\Omega$ into M line segments $\partial\Omega_j$ with endpoints $P_{1,j}$ and $P_{2,j}$, $j = 1, \ldots, M$ (see Figure 1).

For $0 \leqslant t \leqslant 1$, we let (in the piecewise linear instance)

$$\begin{aligned} M_1(t) &= 1 - t, \\ M_2(t) &= t \end{aligned} \tag{14}$$

and, if $P_{i,j} = (x_i^j, y_i^j)$ denotes the Cartesian co-ordinates for the point $P_{i,j}$, we parametrize $\partial\Omega_j$ by

$$\begin{aligned} x(t) &= \sum_{i=1}^{2} M_i(t)x_i^j, \\ y(t) &= \sum_{i=1}^{2} M_i(t)y_i^j. \end{aligned} \tag{15}$$

We then approximate ϕ and $\phi_n \equiv \partial\phi/\partial n$ by

$$\begin{aligned} \tilde{\phi}(Q) &= \sum_{i=1}^{2} \tilde{\phi}(P_{i,j})M_i(t), \\ \frac{\partial\tilde{\phi}}{\partial n}(Q) &= \sum_{i=1}^{2} \tilde{\phi}_n(P_{i,j})M_i(t), \end{aligned} \tag{16}$$

where $Q = Q(t) = \sum_{i=1}^{2} P_{i,j} M_i(t)$. In the Dirichlet problem $\tilde{\phi}(P_{i,j}) = \phi(P_{i,j})$ and the unknowns are $\tilde{\phi}_n(P_{i,j})$. Similarly for the Neumann problem we set $\tilde{\phi}_n(P_{i,j}) = \phi_n(P_{i,j})$ and solve for the unknown $\tilde{\phi}(P_{i,j})$. For Robin or mixed boundary conditions one must choose to eliminate one of $\tilde{\phi}$ or $\tilde{\phi}_n$ in favour of the other.

The integral equation (11) becomes

$$c(P)\tilde{\phi}(P) = \sum_{j=1}^{M} \left\{ \sum_{i=1}^{2} \tilde{\phi}_n(P_{i,j}) \int_{\partial\Omega_j} M_i(t) \log \frac{1}{R_{PQ}} - \sum_{i=1}^{2} \tilde{\phi}(P_{i,j}) \int_{\partial\Omega_j} M_i(t) \frac{\partial}{\partial n_Q} \log \frac{1}{R_{PQ}} \right\}. \tag{11a}$$

Upon collocation at the points $P_{l,m}$ we have

$$c(P_{l,m})\tilde{\phi}(P_{l,m}) = \sum_{j=1}^{M} \left\{ \sum_{i=1}^{2} \tilde{\phi}_n(P_{i,j}) \beta_{i,j}(P_{l,m}) - \sum_{i=1}^{2} \tilde{\phi}(P_{i,j}) \alpha_{i,j}(P_{l,m}) \right\}, \tag{17}$$

where

$$\alpha_{i,j}(P) = \int_{\partial\Omega_j} M_i(t) \frac{\partial}{\partial n_Q} \log \frac{1}{R_{PQ}},$$

$$\beta_{i,j}(P) = \int_{\partial\Omega_j} M_i(t) \log \frac{1}{R_{PQ}}. \tag{18}$$

Because $P_{2,m-1} = P_{1,m}$ (17) contains M independent equations provided that $\tilde{\phi}$ and $\tilde{\phi}_n$ are continuous. If one of them has a discontinuity at some $P_{1,j}$ then $P_{2,j-1}$ contributes an extra equation. For simplicity we shall not consider that case here. For given Neumann boundary conditions, (17) is Fredholm of the second kind, for given Dirichlet conditions it is Fredholm of the first kind. As mentioned above, for Robin boundary conditions one must eliminate one variable in favour of the other.

Finally, we turn to the matrix equation characterizing the linear system. To this end, we note that an effect of discretizing the boundary into linear panels is to introduce non-unique normals at the panel nodes. However, since integration along individual panels is carried out independently of neighbouring panels, this uniqueness problem is circumvented by defining at each node two normals, one for each of the two panels having the node in common.

Define the coefficients $a_{k,j}$ and $b_{k,j}$ by

$$\begin{aligned} a_{k,j+1} &= \alpha_{2,j}(P_k) + \alpha_{1,j+1}(P_k) - \delta_{k,j} c(P_k), \\ b_{k,2j-1} &= \beta_{1,j}(P_k), \\ b_{k,2j} &= \beta_{2,j+1}(P_k), \end{aligned} \tag{19}$$

$k = 1, 2, 3, \ldots, M$, $j = 1, 2, 3, \ldots, M$, where for convenience of notation we set $P_k = P_{2,k}$. For these collocation points P_k, the $\alpha_{i,j}$ and $\beta_{i,j}$ of (18) may be computed analytically. By the assumption of a closed boundary note that

$$\alpha_{1,M+1}(P_k) = \alpha_{1,1}(P_k),$$

and

$$\beta_{1,M+1}(P_k) = \beta_{1,1}(P_k).$$

Thus, equations (17) have the matrix form

$$\mathbf{A}\tilde{\boldsymbol{\phi}} = \mathbf{B}\tilde{\boldsymbol{\phi}}_n, \tag{20}$$

where

$$\mathbf{A} = (a_{k,j}), \quad \mathbf{B} = (b_{k,j}),$$
$$\tilde{\boldsymbol{\phi}} = (\tilde{\phi}(\mathrm{P}_1), \ldots, \tilde{\phi}(\mathrm{P}_M))^{\mathrm{T}}$$

and

$$\tilde{\boldsymbol{\phi}}_n = (\tilde{\phi}_{n_1}(\mathrm{P}_1), \quad \tilde{\phi}_{n_2}(\mathrm{P}_1), \quad \tilde{\phi}_{n_1}(\mathrm{P}_2), \ldots, \tilde{\phi}_{n_1}(\mathrm{P}_m), \quad \tilde{\phi}_{n_2}(\mathrm{P}_m))^{\mathrm{T}}.$$

Note that the subscripts on n_1 and n_2 denote the two normals assigned at each node. To equation (20) we add the constraint

$$\sum_{j=1}^{M} (\tilde{\phi}_{n_1}(\mathrm{P}_j) + \tilde{\phi}_{n_2}(\mathrm{P}_j)) l_j = 0, \tag{21}$$

where l_j denotes the length of the boundary segment $\partial\Omega_j$. This constraint is the discrete analogue of the compatibility condition on the boundary data that follows from $\Delta\phi = 0$. When only Neumann data is present, to guarantee a unique solution, another constraint is needed. We choose to specify the average value of the solution on the boundary, i.e.

$$\sum_{j=1}^{M} \tilde{\phi}(\mathrm{P}_j) l_j = 0. \tag{22}$$

For the Robin boundary condition, we need only the constraint (21). For Step 2 of the solenoidal projection algorithm which is a pure Neumann problem, both constraints are needed.

The matrix equation (20), (22) may be solved for the unknown boundary corrector $\tilde{\phi}_1$ by any appropriate least squares solver. Special domain properties may conceivably enter into this choice. We used a general IMSL subroutine in the calculations given later in this paper.

To complete the corrector Step 2 of the hybrid scheme, we also need $\tilde{\phi}_1$ and $\nabla\tilde{\phi}_1$ at interior points P. The $\tilde{\phi}_1(\mathrm{P})$, and then the $\nabla\tilde{\phi}_1(\mathrm{P})$ by straightforward differences, are obtained from the discretized integral equation (11a). The needed coefficients $\alpha_{i,j}(\mathrm{P})$ and $\beta_{i,j}(\mathrm{P})$ of (18) are obtained by applying a near-field–far-field algorithm described in the next section.

3. NEAR-FIELD–FAR-FIELD INTEGRAL EVALUATIONS

The integrals $\alpha_{i,j}(\mathrm{P})$ and $\beta_{i,j}(\mathrm{P})$ defined in equation (18) for interior points must be evaluated as efficiently as possible. Near-field–far-field techniques have been developed for aerodynamics codes for this purpose. We refer to Reference 8 for a discussion of source far-field evaluations and to Reference 9 for doublets and higher order sources.

Briefly, the idea is that if P is far enough away from the panel or boundary segment in question, the integrals are very nearly the same as the influence of point sources, point dipoles, higher order moments, or a combination of the above depending on the accuracy desired. Traditionally, these moments have been placed at the panel or boundary segment centre. The approach given here uses only point charges to approximate both source and dipole distributions and allows for their placement to be off the panel. This generalizes previous formulations and is crucial to the use of fast direct methods in evaluating the $\alpha_{i,j}(\mathrm{P})$ and $\beta_{i,j}(\mathrm{P})$ cheaply.

If the point P is close to the panel in question a more accurate evaluation is required. The choice of panels or linear segments in approximating boundary arcs along with more general polynomial singularity distributions allows for the analytic evaluations of these integrals as described by Johnson and Rubbert.[9] Various weighted quadrature techniques have also been used, for instance Fairweather *et al.*[24] use Gaussian quadrature on quadratic boundary arcs. In the latest generation of aerodynamics codes, different methods are used depending on the distance

between the panel and the point P. In many cases 90 per cent of the integral evaluations are performed by far-field routines, reducing computing times by an order of magnitude.

Here we give error estimates for a general far-field approximation method that is shown to be first order accurate.

Let the fixed point P be denoted by (P_1, P_2), and let the variable boundary point Q be parametrized by $Q(t) = (X(t), Y(t))$. Then, noting that

$$\frac{\partial}{\partial n_Q} \log 1/R_{PQ} = -n_Q \cdot \frac{P-Q}{R_{PQ}^2} = -\left\{\frac{d}{dt} \tan^{-1}\left[\frac{Y(t)-P_2}{X(t)-P_1}\right]\right\} \cdot \frac{1}{(X'(t)^2 + Y'(t)^2)^{1/2}} \tag{23}$$

and letting $\theta(P, Q(t))$ denote the angle defined by the inverse tangent in (23), we have from (18) the expressions

$$\alpha_{i,j}(P) = -\int_0^1 M_i(t) \frac{\partial \theta(P, Q(t))}{\partial t} dt, \tag{24}$$

$$\beta_{i,j}(P) = -\int_0^1 M_i(t) \left[\log \frac{1}{R_{PQ(t)}}\right] (X'(t)^2 + Y'(t)^2)^{1/2} dt.$$

For a given boundary element these quantities may be analytically evaluated. For far-field approximations, one essentially uses Newton's concept that a set of charges at a distance appears as a single charge at a centroid point. The $\alpha_{i,j}(P)$ and $\beta_{i,j}(P)$ are approximated using discrete charges at grid points of the superimposed rectangular grid.

Consider the source integral $\beta_{i,j}(P)$. Let Q_0 be the grid point closest to the centre of the boundary element (see Figure 2). Let $R_0 = R_{P,Q_0}$ be the vector between P and Q_0, and let $\Delta R = R_{PQ} - R_0$. Let the grid points be spaced a distance h apart in both the x and y directions. Expanding $\log 1/R$ in a Taylor series, where now R denotes the scalar $|R_{PQ}|$,

$$\log \frac{1}{R} = \log \frac{1}{|R_0|} - (R_0, \Delta R)/|R_0|^2 + \cdots$$

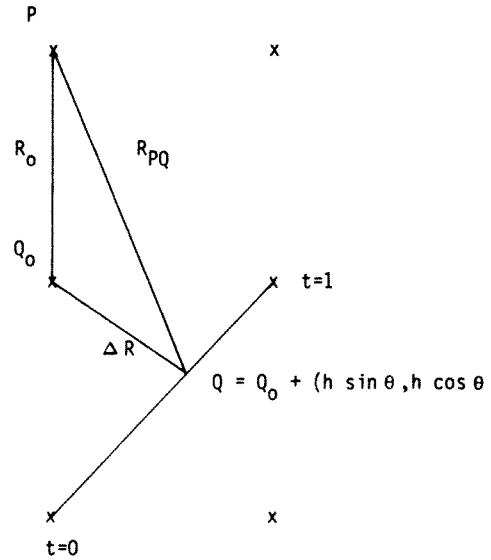

Figure 2(a). 45° panel orientation geometry

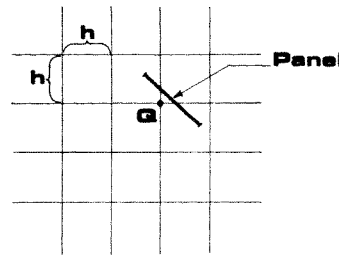

Figure 2(b). Point charge representation of a source panel

Placing a single charge of strength $\sigma = \int_{\partial\Omega_j} M_i \, ds$ at Q_0 and keeping only the lowest order error term,

$$\left|\beta_{i,j}(P) - \sigma \log \frac{1}{|R_0|}\right| \leqslant \left|\int_{\partial\Omega_j} M_i \frac{(R_0, \Delta R)}{|R_0|^2} ds\right| + \text{higher order terms.}$$

Let l be the length of the boundary element $\partial\Omega_j$. For error estimation we further require that the panel length be smaller than some constant multiple of the grid spacing h. Then

$$\begin{aligned}\left|\int_{\partial\Omega_j} M_i \frac{(R_0, \Delta R)}{|R_0|^2} ds\right| &\leqslant \frac{1}{|R_0|} \int_{\partial\Omega_j} |M_i||\Delta R| \, ds \\ &\leqslant K_1 l^2/|R_0| \leqslant K_2 h^2/|R_0|,\end{aligned}$$

where K_2 depends on $\int_{\partial\Omega_j} M_i \, ds$, i.e. the strength of the singularity distribution, the constant relating panel length l and grid spacing h, and on the orientation of the panel.

For example, if the panel is oriented at 45° to the grid lines and is of length $h\sqrt{2}$ then

$$\int_{\partial\Omega_j} M_i \frac{(R_0, \Delta R)}{|R_0|^2} ds = \int_0^1 (1-t)(\cos\theta) \frac{(R_0)(\Delta R)}{2R_0^2 h} dt = (h^2\sqrt{2}/R_0) \int_0^1 -(t-1)^2 \, dt = -h^2\sqrt{2}/(3R_0).$$

Hence, in this case the constant K_2 has the value $-\sqrt{2}/3$.

The $\alpha_{i,j}(P)$ are approximated similarly by using a discrete dipole consisting of three charges at grid points as described by Proskurowski and Widlund[13] (see Figure 3). In this case the principal error term is $K_3 h^2/R_0^2 + K_4 h^2/R_0^3$ where K_3 and K_4 depend on the strength of the dipole distribution, the constant relating panel length l to the grid spacing h, and on the orientation of the panel.

Since in two dimensions there are $O(1/h)$ panels on a fixed boundary curve, the overall error is first order in h at a fixed distance from the boundary. Higher order can be achieved by taking

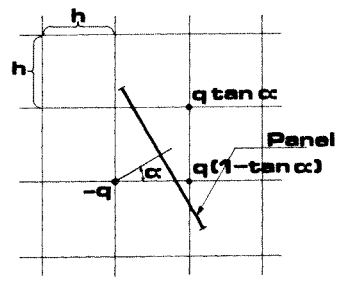

Figure 3. Discrete dipole representation of a dipole panel using three charges

more terms in the expansions and using more discrete charges per panel as in Reference 25. Furthermore, a global second order scheme may be achieved provided each boundary element contains a node of a bisecting, normal grid line. Under such conditions the local error is third order in h. This is the case, for instance, for any region which is a union of rectangles aligned with the grid. For a locally second order method for the source layer, we require that $K_2 h^2/R_0 \leqslant h^2$. Thus a suitable cut-off criterion would be to use accurate near-field calculations whenever $R_0 \leqslant K_2$, and efficient far-field calculations otherwise. Similar estimates can be made for the dipole layer.

The potential $\tilde{\phi}_1(\mathrm{P})$ at interior points P for Step 2 of our scheme is thus computed at reduced cost by use of the far-field approximation outlined here. Its implementation needs only one call to a fast direct solver (e.g. FFT enhanced convolution routine) which does all panels simultaneously.

For uniform high order accuracy one can use the more accurate near field influences for panel/point pairs that are close together. This correction process can be made inexpensive compared to the fast direct solver itself. More details of this correction process can be found in Reference 25.

The crucial point about the method given above is that the effect of the boundary singularities can be accurately simulated on a rectangular grid of points provided that near-field corrections are used. This allows the use of fast direct methods or multigrid methods to reduce the cost of computation.

In Section 5 one will find both far-field (see Figures 5–7 and Tables I, II) and near-field (see Figure 8) computations.

4. SYMMETRY, CAPACITANCE MATRICES, OPERATION COUNTS AND RELATED CONSIDERATIONS

In this section we consider a number of related analytical questions. A main idea is that the more symmetrical the domain Ω, the more amenable it is to the efficient or even analytical inversion of the fundamentally important matrix equation (20). In particular, we illustrate, by means of the Dirichlet and Neumann problems for a regular n-gon, the role of symmetry and a connection to the theory of capacitance matrices. Consider the linear system coming from the boundary integral equation for a circular region Ω. An optimal way of linearizing a circle is by using inscribed regular n-gons (see Figure 4). As shown above, the matrix equation representing this system is given by (20) along with the compatibility constraints (21) or (22). Matrices arising from the

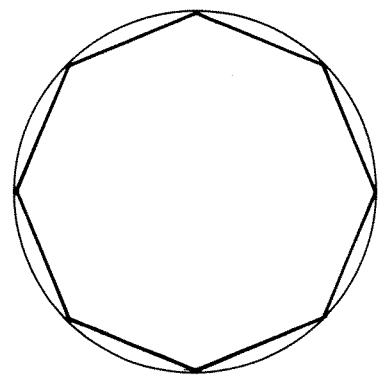

Figure 4. Octagon inscribed in a unit circle

discretization of boundary integral equations on regular n-gons are highly symmetric, and, in fact, are cyclic. This makes them amenable to Fourier analysis.

Let us first note some interesting properties of the matrices **A** and **B** of equation (20) corresponding to this region. Symmetry of the domain dictates that $\alpha_{i,j}(P_{k+1}) = \alpha_{i,j-1}(P_k)$, and $\beta_{i,j}(P_{k+1}) = \beta_{i,j-1}(P_k)$, where the P_k represent the vertices of the regular n-gon. Since $c(P_k) = c(P_{k+1})$, it follows from (19) that $a_{k,j-1} = a_{k+1,j}$ and $b_{k,j-1} = b_{k+1,j}$. Thus the matrices **A** and **B** of (20) are both cyclic. In addition

$$\sum_{j=1}^{n} a_{k,j} = \sum_{j=1}^{n} \int_{\partial\Omega_j} \frac{\partial}{\partial n_Q} \log R_{P_kQ} - c(P_k)$$

and from

$$c(P_k) = \int_{\partial\Omega} \frac{\partial}{\partial n_Q} \log R_{P_kQ} = \sum_{j=1}^{n} \int_{\partial\Omega_j} \frac{\partial}{\partial n_Q} \log R_{P_kQ},$$

we see that

$$\sum_{j=1}^{n} a_{k,j} = 0, \quad k = 1, \ldots, n. \tag{25}$$

Since

$$\frac{\partial}{\partial n_Q} \log R_{P_kQ} = \frac{-\cos(\overline{P_kQ}, n_Q)}{R_{P_kQ}},$$

we see, in addition, that $a_{k,j} > 0$ for $k \neq j$. Here $\overline{P_kQ}$ is the vector representing the line segment joining the points P_k and Q. Finally, $a_{k,k} = -c(P_k)$.

Thus the augmented matrix equation (i.e. (20) with constraints (21) or (22)) for the boundary integral equation (17) on a regular n-gon has the form

$$\bar{\mathbf{A}}\tilde{\boldsymbol{\phi}} = \bar{\mathbf{B}}\tilde{\boldsymbol{\phi}}_n, \tag{26}$$

where $\bar{\mathbf{A}}$ and $\bar{\mathbf{B}}$ are the $(n+1) \times n$ and $(n+1) \times 2n$ matrices

$$\bar{\mathbf{A}} = \begin{bmatrix} \mathbf{A}_{n\times n} \\ l\mathbf{I}_{1\times n} \end{bmatrix}, \quad \bar{\mathbf{B}} = \begin{bmatrix} \mathbf{B}_{n\times 2n} \\ l\mathbf{I}_{1\times 2n} \end{bmatrix},$$

where $\mathbf{I}_{1\times n} = (1, 1, \ldots, 1)$ and l is a constant equal to the length of the sides of the inscribed regular n-gon.

We next show how to solve the Neumann problem efficiently. To achieve this we sketch a procedure for inverting the matrix $\bar{\mathbf{A}}$ of equation (26).

The left inverse of $\bar{\mathbf{A}}$ will be of the form

$$\bar{\mathbf{A}}^{-1} = [\mathbf{D}_{n\times n} \quad \mathbf{I}_{n\times 1}], \tag{27}$$

where $\mathbf{I}_{n\times 1} = (1, 1, \ldots, 1)^{\mathrm{T}}$. The matrix $\mathbf{D}_{n\times n}$ is itself cyclic and so will be fully determined once its first row is known. This first row $\mathbf{X}^{\mathrm{T}}$ of $\mathbf{D}_{n\times n}$ satisfies the equation

$$\mathbf{X}^{\mathrm{T}}\bar{\mathbf{A}} = \mathbf{b}^{\mathrm{T}}, \tag{28}$$

where $\mathbf{b}^{\mathrm{T}} = (1-l, -l, \ldots, -l)$. Letting λ_j, $j = 0, \ldots, n-1$ denote the components of the discrete Fourier transform of the first row of $\bar{\mathbf{A}}^{\mathrm{T}}$, it can be seen that for $j \neq 0$, $\lambda_j \neq 0$

$$\mathbf{X}^{\mathrm{T}} = \sum_{j=1}^{n-1} \frac{1}{n\lambda_j} \mathbf{W}_n^j, \tag{29}$$

where

$$\mathbf{W}_n^j = \left(1, \exp\left(\frac{2\pi ij}{n}\right), \ldots, \exp\left(\frac{2\pi ij(n-1)}{n}\right)\right)^{\mathrm{T}}$$

(for details, see Reference 26). Thus, for such regions, the boundary integral equation at the collocation points may be solved by means of discrete Fourier transforms.

The example above reduced to solving an equation of the form

$$\tilde{\boldsymbol{\phi}} = \bar{\mathbf{A}}^{-1}\bar{\mathbf{B}}\tilde{\boldsymbol{\phi}}_n. \tag{30}$$

If we write it in the other direction

$$\tilde{\boldsymbol{\phi}}_n = \bar{\mathbf{B}}^{-1}\bar{\mathbf{A}}\tilde{\boldsymbol{\phi}}, \tag{31}$$

we may regard $\bar{\mathbf{B}}^{-1}$ as a capacitance matrix. Recall that the electrostatic capacity proportions charge and potential according to $Q = CV$. In our case $\tilde{\boldsymbol{\phi}}_n$ represents charge sources and $\bar{\mathbf{A}}\tilde{\boldsymbol{\phi}}$ a potential. We mention in making this connection that our interpretation agrees with the convention of Hockney[22] but we hasten to add that in much of the capacitance matrix literature, the capacitance matrix corresponds to C^{-1}.

Let us next turn to the issue of calculating a discrete Green's function for a given region. In particular, consider the problem of placing only source charges at collocation points along the boundary of a region in such a way as to enforce a Dirichlet boundary condition at those points. Assuming that such a charge distribution could be found, it would then be possible to compute the resulting potential field by convolving the source distribution with the influence function $S = -(1/2\pi)\log R$. Thus, letting $\mathbf{f}$ denote the vector consisting of the boundary conditions at the collocation points, we see that the vector of source charges for the collocation points must satisfy the matrix equation

$$\mathbf{Cq} = \mathbf{f}.$$

The domain potential is found by

$$\phi = S * T\mathbf{C}^{-1}\mathbf{f}$$

where T represents the assignment of charges of the one dimensional array $\mathbf{C}^{-1}\mathbf{f}$ to the corresponding nodal positions on $\partial\Omega$ in the two dimensional grid. Provided that $\mathbf{C}^{-1}$ exists, a discrete Green's function for the domain is

$$G = S * T\mathbf{C}^{-1}.$$

The investigation of the question of inverting $\mathbf{C}$ for general domains is an interesting problem. However, for highly symmetric domains such as the regular n-gon, the matrix $\mathbf{C}$ becomes more amenable to analysis. In the case of a regular n-gon, with the collocation points being the vertices themselves, it can be shown that $\mathbf{C}$ is cyclic and, moreover, is invertible provided that the discrete Fourier transform of its first row has no zero components. Numerical tests for several values of n have shown this always to be the case.

The use of sources only in computing domain potentials has the advantage that it is often easier to place them in ideal locations (i.e. near the middle of a panel) which is not the case for the placement of dipoles. We next turn our attention to an operation count in two dimensions for the hybrid scheme. Let N be the number of grid lines, in each direction, of the rectangular domain Ω' containing the region Ω of the problem. Let P be the number of linear segments (i.e. panels) used to approximate $\partial\Omega$. Then

1. To solve equation (12) for ϕ_3 by fast direct methods requires $O(N^2 \log_2 N)$ operations.
2. To interpolate ϕ_3 onto the $P = O(N)$ collocation points of $\partial\Omega$ requires $O(N)$ operations.

3. To solve the boundary integral equation, as the linearized matrix equation (20), requires $O(N^3)$ operations, if done directly.
4. To compute $\phi_1(P)$, equation (13), for far-field points P, entails $O(N^2 \log_2 N)$ operations.
5. Finally, to compute $\phi_1(P)$, equation (13) for near-field points P requires $O(N^3)$ operations.

Note that we do not include in our operation count the construction of the matrices representing the linearization of the boundary integral equations. Such matrices depend on the geometry of the domain only and, hence, may be precomputed. In addition, the large count for the inversion of the linear system may be attenuated with respect to the other counts whenever many calls to the solver are needed for a fixed domain. Our examples show this operation count is very conservative. The cost of the near field computations can be reduced by using higher order approximations for $\alpha_{i,j}$ and $\beta_{i,j}$ as given in Reference 25.

In three dimensions, the far-field error can be estimated by expanding $1/R$ in a Taylor series as in Section 3. The corresponding error term for source distributions is Kh^3/R_0^3. Since the number of panels P is $O(N^2)$, the operation counts are

1. $O(N^3 \log N)$ to find ϕ_3.
2. $O(N^2)$ to do the required interpolation onto the collocation points
3. to solve (20) directly requires $O(N^6)$ operations
4. to compute $\phi_1(P)$ at far-field points P requires $O(N^3 \log N)$ operations
5. to compute the near-field corrections for $\phi_1(P)$ requires $O(N^5)$ operations with a large constant.

Iterative methods such as those studied in Reference 25 can reduce the counts for 3 and 5 to $O(N^3 \log N)$ operations.

5. NUMERICAL RESULTS

Both far-field and near-field computations were performed to test the method. We present results for rectangles, triangles, diamonds, pentagons, octagons and L-shaped regions. Panel lengths were proportional to the width of a grid box for all the runs. The error estimates indicate that this increases the order of convergence. First, in testing Step 2 of our scheme, we limited ourselves to the far-field, i.e. uncorrected, method. However, the far-field solution was quite accurate even very close to the boundary as shown in Figures 5–7 and Tables I–III. An exception to this is the missing entries in Figures 5 and 6, where the exponents were non-negative. In all of these cases, we used the functions $\phi(x, y) = x - y$, and $\phi(x, y) = x^2 - y^2$, as the test cases. The length and width of a grid box is denoted by h. The enclosing rectangular region, in all cases, is the unit square. The problem treated was the recovery of ϕ from its known boundary values ϕ and $\partial\phi/\partial n$, by use of far-field methods applied to (11a).

Secondly, we tested the boundary integral solution of (20), (22) for $\tilde{\phi}_1$ at the boundary nodes. These were found to be second order accurate, see Table III.

Finally, we illustrate the full solenoidal algorithm on a square and on an L-shaped region, employing the more accurate near-field methods (see Figure 8).

```
      -LOG2(ABSOLUTE ERROR) BEFORE CORRECTION
                  4
               5  6  4
               2  5  1
               5 12  3
               3  7  1
               8  9  4
      5  2  5  3 848  8  2
   4  6 512  7  9 847  5
      4  1  3  1  4  2 551
```

Figure 5(a). $-\log_2$ (error) of the far field method at all interior points of an L-shaped region with mesh size $h = 1/10$ and panel length $l = 2h$. Twenty panels in all. Test function $\phi = x - y$

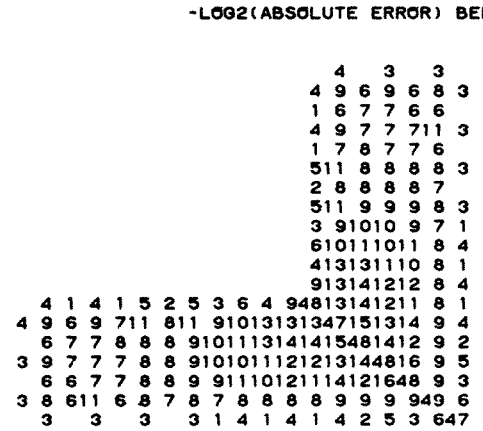

Figure 5(b). $-\log_2$ (error) of the far field method at all interior points of an L-shaped region with mesh size $h = 1/20$ and panel length $l = 2h$. Forty panels in all. Test function $\phi = x - y$

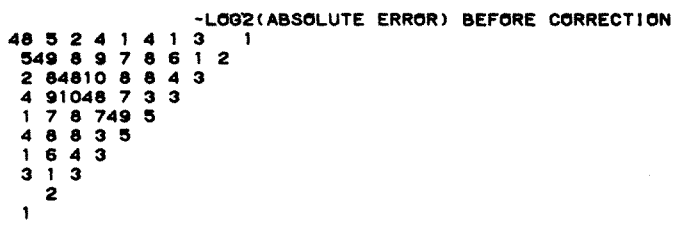

Figure 6(a). $-\log_2$ (error) of the far field method at all interior points of a right triangle with mesh size $h = 1/12$ and panel length $l = 2h$. 18 panels in all. Test function: $\phi = x - y$

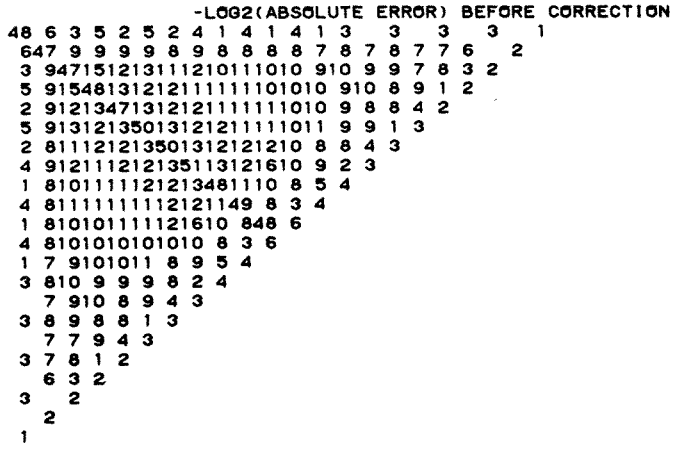

Figure 6(b). $-\log_2$ (error) of the far field method at all interior points of a right triangle with mesh size $h = 1/24$ and panel length $l = 2h$. 36 panels in all. Test function: $\phi = x - y$

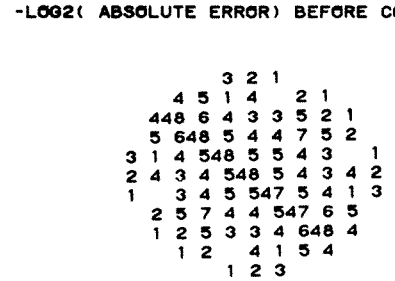

Figure 7(a). $-\log_2$ (error) of the far field method at all interior points of the unit octagon with mesh size $h = 1/14$ and one panel per side. Test function $\phi = x - y$

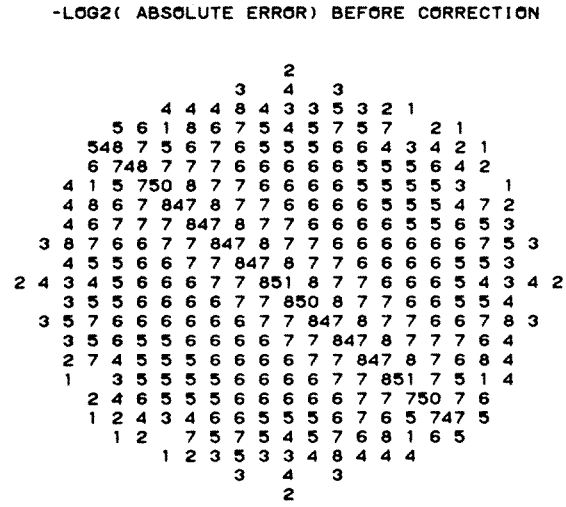

Figure 7(b). $-\log_2$ (error) of the far field method at all interior points of the unit octagon with mesh size $h = 1/28$ and two panels per side. Test function $\phi = x - y$

Table I. $-\log_2$ (absolute error) at the far field point P = (0·625, 0·500) versus mesh size h for the test function $x - y$

h	Equilateral triangle	Diamond (square)	Pentagon	Octagon	L-shaped region
1/32	5	7	7	7	13
1/64	6	10	9	10	15
1/128	9	12	9	10	17
1/256	11	12	11	10	19
1/512	11	13	12	11	21
1/1024	12	15	13	13	23
1/2048	14	16	14	14	

Table II. $-\log_2$ (absolute error) at the far field point P = (0·625, 0·500) versus mesh size h for the test function $x^2 - y^2$

h	Equilateral triangle	Diamond (square)	Pentagon	Octagon	L-shaped region
1/32	4	7	7	7	14
1/64	6	9	9	10	16
1/128	10	13	9	10	18
1/256	11	12	10	9	20
1/512	11	13	12	11	22
1/1024	13	14	12	13	24
1/2048	14	16	13	13	

Figures 5–7 and Tables I, II indicate that for relatively small mesh sizes (i.e. $h \leqslant 1/64$) the convergence rate is first order, in agreement with the estimates of Section 3 above.

Next, in Table III we show that the discretization of the boundary integral equation by linear elements without far-field approximations, i.e. equation (20), is second order in h. The harmonic functions $\phi(x, y) = \mathrm{Re}\, Z^k$ were used as solutions to the Dirichlet problem on domains Ω_n = the regular n-gon inscribed in the unit circle.

Table III. Discretization of boundary integral equation using linear approximations. The domain is a regular n-gon inscribed in the unit circle. Entries are relative errors. Test function $\phi(x, y) = \mathrm{Re}\, Z^k$

	$n = 10$	$n = 20$	$n = 40$
$k = 1$	0·086	0·003	0·001
$k = 2$	0·225	0·015	0·004
$k = 3$	0·342	0·039	0·011

We close this section with two examples of solenoidal projection according to the algorithm of Section 1 and employing the hybrid method of Section 2. The two domains considered are a square and an L-shaped region. In both cases the test vector field is $\mathbf{v} = (x, y)$ and in both cases a total of twenty panels, each of length 0·2, were used to discretize the boundary. Figures 8(a) and 8(b) give the x and y components of the projection v_2 at all grid nodes of the regions, as well as their respective discrete divergence values at all interior grid nodes. The notation is $v_2 = \mathrm{V2} = (\mathrm{VX2}, \mathrm{VY2})$.

THE 11 BY 11 MATRIX IS VX2

0	-.873E-01	-.548E-01	-.104E-01	-.838E-02	-.323E-02	.116E-02	.241E-02	.295E-01	.448E-01	0
0	-.512E-01	-.210E-01	-.125E-01	-.697E-02	-.355E-02	-.761E-03	.253E-02	.685E-02	.132E-01	0
0	-.240E-01	-.106E-01	-.840E-02	-.557E-02	-.324E-02	-.144E-02	-.207E-03	-.656E-03	-.135E-01	0
0	-.552E-02	-.420E-02	-.450E-02	-.356E-02	-.243E-02	-.163E-02	-.163E-02	-.337E-02	-.181E-01	0
0	-.102E-01	-.100E-02	-.169E-02	-.165E-02	-.129E-02	-.108E-02	-.146E-02	-.268E-02	-.357E-03	0
0	.803E-02	.148E-02	.281E-03	-.712E-04	.568E-13	.712E-04	-.281E-03	-.148E-02	-.803E-02	0
0	.357E-03	.268E-02	.146E-02	.108E-02	.129E-02	.165E-02	.169E-02	.100E-02	.102E-01	0
0	.181E-01	.337E-02	.163E-02	.163E-02	.243E-02	.356E-02	.450E-02	.420E-02	.552E-02	0
0	.135E-01	.656E-03	.207E-03	.144E-02	.324E-02	.557E-02	.840E-02	.106E-01	.240E-01	0
0	-.132E-01	-.685E-02	-.253E-02	.761E-03	.355E-02	.697E-02	.125E-01	.210E-01	.512E-01	0
0	-.448E-01	-.295E-01	-.241E-02	-.116E-02	.323E-02	.838E-02	.104E-01	.548E-01	.873E-01	0

THE 11 BY 11 MATRIX IS VY2

0	0	0	0	0	0	0	0	0	0	0
.746E-01	.433E-01	.113E-01	-.891E-03	.931E-02	-.370E-02	.932E-02	-.110E-02	.119E-01	.291E-01	.702E-01
.543E-01	.196E-01	.864E-02	.276E-02	.615E-03	-.652E-03	-.504E-03	.218E-03	.366E-02	.104E-01	.350E-01
.222E-01	.138E-01	.841E-02	.423E-02	.171E-02	.310E-03	-.246E-03	-.470E-04	.100E-02	.197E-02	-.122E-01
.202E-01	.953E-02	.659E-02	.386E-02	.181E-02	.373E-03	-.624E-03	-.133E-02	-.197E-02	-.322E-02	-.120E-01
.150E-01	.641E-02	.444E-02	.273E-02	.129E-02	.320E-13	-.129E-02	-.273E-02	-.444E-02	-.641E-02	-.150E-01
.120E-01	.322E-02	.197E-02	.133E-02	.624E-03	-.373E-03	-.181E-02	-.386E-02	-.659E-02	-.953E-02	-.202E-01
.122E-01	-.197E-02	-.100E-02	.470E-04	.246E-03	-.310E-03	-.171E-02	-.423E-02	-.841E-02	-.136E-01	-.222E-01
-.350E-01	-.104E-01	-.366E-02	-.218E-03	.504E-03	.652E-03	-.615E-03	-.276E-02	-.864E-02	-.196E-01	-.543E-01
-.702E-01	-.291E-01	-.119E-01	.110E-02	-.932E-02	.370E-02	-.931E-02	.891E-03	-.113E-01	-.433E-01	-.746E-01
0	0	0	0	0	0	0	0	0	0	0

THE 9 BY 9 MATRIX IS DIV(V2)

.203E+00	.150E+00	.566E-01	.418E-01	.343E-01	.329E-01	.370E-01	.352E-01	-.864E-01
.948E-01	.922E-01	-.617E-03	.638E-01	.634E-03	.630E-01	-.137E-02	-.119E-01	.139E+00
.294E-01	.153E-01	-.231E-02	.439E-02	.451E-02	.461E-02	-.963E-03	-.541E-01	.852E-01
.319E-01	.625E-01	.419E-02	.405E-02	.442E-02	.441E-02	.546E-02	.327E-01	.553E-01
.389E-01	-.157E-01	.491E-02	.452E-02	.444E-02	.452E-02	.491E-02	-.157E-01	.389E-01
.553E-01	.327E-01	.546E-02	.441E-02	.442E-02	.405E-02	.419E-02	.625E-01	.319E-01
.852E-01	-.541E-01	-.963E-03	.461E-02	.451E-02	.439E-02	-.231E-02	.153E-01	.294E-01
.139E+00	-.119E-01	-.137E-02	.630E-01	.634E-03	.638E-01	-.617E-03	.922E-01	.948E-01
-.864E-01	.352E-01	.370E-01	.329E-01	.343E-01	.418E-01	.566E-01	.150E+00	-.203E+00

Figure 8(a). Solenoidal projection of $\mathbf{V} = (x, y)$ onto a unit square. The panel length is 0·2. The top two matrices correspond to the x and y-components, respectively. The third matrix gives values of the discrete divergence of the projected vector at interior nodes

THE 11 BY 11 MATRIX IS VX2

0	-.783E-01	-.497E-01	-.930E-02	-.824E-02	-.404E-02	-.330E-03	.244E-03	.238E-01	.355E-01	0
0	-.451E-01	-.188E-01	-.117E-01	-.716E-02	-.442E-02	-.219E-02	.478E-03	.401E-02	.662E-02	0
0	-.213E-01	-.973E-02	-.842E-02	-.623E-02	-.433E-02	-.285E-02	-.190E-02	-.245E-02	-.164E-01	0
0	-.371E-02	-.466E-02	-.566E-02	-.491E-02	-.383E-02	-.306E-02	-.308E-02	-.467E-02	-.207E-01	0
0	-.874E-02	-.371E-02	-.446E-02	-.380E-02	-.297E-02	-.254E-02	-.280E-02	-.382E-02	-.268E-02	0
0	-.457E-02	-.593E-02	-.457E-02	-.277E-02	-.164E-02	-.133E-02	-.164E-02	-.266E-02	-.105E-01	0
0	-.273E-01	-.235E-01	-.636E-02	0	.161E-02	.417E-03	.142E-03	-.417E-03	.773E-02	0
				0	.164E-02	.202E-02	.231E-02	.220E-02	.243E-02	0
				0	.524E-02	.219E-02	.479E-02	.748E-02	.205E-01	0
				0	-.186E-01	-.414E-03	.704E-02	.164E-01	.440E-01	0
				0	-.188E-01	-.567E-02	.431E-02	.468E-01	.775E-01	0

THE 11 BY 11 MATRIX IS VY2

0	0	0	0	0	0	0	0	0	0	0
.644E-01	.356E-01	.748E-02	-.434E-02	.660E-02	-.635E-02	.690E-02	-.383E-02	.904E-02	.224E-01	.609E-01
.462E-01	.144E-01	.487E-02	.185E-03	-.120E-02	-.207E-02	-.179E-02	-.119E-02	.176E-02	.750E-02	.291E-01
.162E-01	.716E-02	.361E-02	.114E-02	-.350E-03	-.129E-02	-.172E-02	-.160E-02	-.809E-03	-.224E-03	-.145E-01
.315E-03	-.228E-03	.118E-02	.104E-02	.930E-04	-.109E-02	-.209E-02	-.283E-02	-.353E-02	-.485E-02	-.137E-01
-.167E-01	-.206E-01	-.859E-04	-.885E-03	.181E-02	-.120E-02	-.277E-02	-.416E-02	-.571E-02	-.756E-02	-.161E-01
0	0	0	0	0	-.193E-02	-.360E-02	-.528E-02	-.755E-02	-.101E-01	-.205E-01
				-.669E-03	-.391E-02	-.430E-02	-.569E-02	-.894E-02	-.136E-01	-.217E-01
				-.241E-01	-.647E-02	-.387E-02	-.403E-02	-.860E-02	-.182E-01	-.501E-01
				-.342E-01	-.668E-02	-.102E-01	.119E-02	-.969E-02	-.382E-01	-.667E-01
				0	0	0	0	0	0	0

THE 9 BY 9 MATRIX IS DIV(V2)

-.166E+00	.142E+00	.575E-01	.425E-01	.352E-01	.334E-01	.369E-01	.219E-01	-.575E-01
.937E-01	.837E-01	-.997E-02	.552E-01	-.844E-02	.552E-01	-.916E-02	-.232E-01	.125E+00
.497E-01	.866E-02	-.554E-02	.273E-02	.435E-02	.527E-02	.169E-03	-.618E-01	.851E-01
.120E+00	.399E-01	.967E-02	-.332E-02	.587E-02	.606E-02	.642E-02	.251E-01	.558E-01
-.308E-01	.594E-02	.210E-01	.151E-01	.114E-01	.753E-02	.559E-02	-.243E-01	.397E-01
				.156E-01	.323E-03	.348E-02	.541E-01	.322E-01
				.328E-01	.471E-02	-.539E-02	.587E-02	.295E-01
				.248E-01	.271E-01	-.795E-02	.823E-01	.656E-01
				-.344E-01	.109E+00	.639E-01	.142E+00	-.173E+00

Figure 8(b). Solenoidal projection of the vector $\mathbf{V} = (x, y)$ onto an L-shaped region. The panel length is 0·2. The top two matrices correspond to the x and y-components, respectively. The third matrix gives values of the discrete divergence of the projected vector at interior nodes

6. NAVIER–STOKES EQUATIONS

For studying numerically the viscous incompressible Navier–Stokes equations

$$\mathbf{v}_t - \frac{1}{Re}\nabla^2\mathbf{v} + (\mathbf{v}\cdot\nabla)\mathbf{v} = -\nabla p + f, \quad \text{in } \Omega, \tag{32}$$

$$\nabla\cdot\mathbf{v} = 0, \quad \text{in } \Omega, \tag{33}$$

on general regions Ω under appropriate boundary conditions on $\partial\Omega$, one encounters, not unsurprisingly, two problems:

1. How should one efficiently solve the momentum equation (32) over a large number, e.g. in the thousands or tens of thousands, of time steps?
2. How can one effectively guarantee that the evolving vector flow field $\mathbf{v}$ remain in the solonoidal subspace, i.e. satisfy (33), at every time step?

The relationships of these two problems and their interplay one with the other are well known and in recent years a number of 'splitting' schemes have been proposed and investigated. We refer the reader to the excellent discussion of these methods given by Peyret and Taylor.[27]

In such methods, in following either a primitive variables (pressure, velocity) formulation or a vorticity–stream-function formulation, one arrives, even after clever tricks such as those of Reference 4, at the need for fast Poisson solvers at each remaining time step. The hybrid scheme of Section 2 is ideally suited to these Navier–Stokes problems for general regions.

Note that most of the finite difference methods described in Reference 27 presume a, locally at least, rectangular boundary $\partial\Omega$. This brings us to three interesting questions.

First, for irregular boundaries treated in a finite difference scheme, as in our use of fast direct methods in the hybrid method for the domain contributions, how does one express the discrete solenoidal condition so as to avoid generating spurious pressures, flow instabilities or mass creation at $\partial\Omega$. For regular regions these matters have been subjected to considerable analysis in a number of references already cited. In particular, the factorization

$$L = DG, \tag{34}$$

L the discrete Laplacian, D the discrete divergence, G the discrete gradient, is quite important to their understanding. Let us recall very quickly why.

Consider a simple marching scheme such as explicit Euler, in which the velocity field is advanced according to

$$\mathbf{v}_{n+1} = \mathbf{v}_n - (G\mathbf{p}_n)\Delta t + F(\mathbf{v}_n)\Delta t, \tag{35}$$

where $F(\mathbf{v}_n)$ denotes the remaining terms in the momentum equation (32). Then

$$D\mathbf{v}_{n+1} = D\mathbf{v}_n - (DG\mathbf{p}_n - DF(\mathbf{v}_n))\Delta t \tag{36}$$

and $\mathbf{v}_{n+1}$ is discretely solenoidal provided that $\mathbf{v}_n$ was discretely solenoidal (one can allow the D's to depend on n) and provided that in the Poisson solver used to compute $\mathbf{p}_n$, namely

$$L\mathbf{p}_n = DF(\mathbf{v}_n), \tag{37}$$

one has consistently factorized as in (34).

Note that it is the case that the MAC, i.e. marker and cell, grid satisfies the factorization (34) that permits the use of fast direct Poisson solvers for adjusting the pressure field at each time step. Likewise in the finite element formulations, e.g. of References 4 and 5, it is the factorization

used there, namely

$$L = \mathbf{C}^{\mathrm{T}}\mathbf{M}^{-1}\mathbf{C}, \tag{38}$$

wherein $\mathbf{C}$ and $\mathbf{C}^{\mathrm{T}}$ denote discrete gradient and divergence, which preserves the mass. The same guiding requirement can be found in most of the methods discussed in Reference 27. Although we have given a preliminary analysis of aspects of this question for irregular Ω in Reference 28 observing in particular the importance of requiring that the flow velocity field have vanishing normal components at the boundary, a more complete analysis of boundary incompressibility consistent with factorizations such as (34) for general domains is needed. If such factorizations cannot be obtained, one could investigate other, albeit less direct, pressure adjustment schemes, in which, for instance, one relaxes the requirement of high precision incompressibility to just incompressibility to some acceptable, e.g. 2nd, order.

The second question is an extension of the first, and brings us full circle to the statement at the end of the Introduction. How should one consistently interface a domain factorization such as (34) with the boundary panel configuration? A third question for the hybrid method is: how should the dipoles and monopoles be placed in the $\alpha_{i,j}$ and $\beta_{i,j}$ calculations to effect a scheme with a consistent factorization near and at the boundary?

7. CONCLUSION

We have investigated a new method for the calculation of solenoidal vector fields on arbitrary regions. Its core is a hybrid Poisson solver combining fast direct methods and boundary elements. Additionally, it employs far field panel methods (compare, for instance, Reference 29: the boundary integral method corresponds to using only near-field formulations) for greater efficiency. It has been tested on several domains and is second order locally and first order globally. A number of interesting related questions have been raised.

ACKNOWLEDGEMENT

The authors appreciate the co-operation of the Boeing Company and the University of Colorado which made possible this endeavour. The last named author appreciates many useful discussions with Forrester Johnson and Malcolm James of the Boeing Company. Computing Resources supplied by the University of Colorado and an NCAR Computing Resources Grant. Partially supported by NSF grant MCS 80-12220. D. P. Young is also partially supported by the Boeing Internal Research and Development Program.

REFERENCES

1. K. Gustafson, 'Estimation of eigenvalue aggregates determining hydrodynamic stability', *Notices Amer. Math. Soc.*, **23**, A-682 (1976).
2. K. Gustafson and D. P. Young, 'Computation of solenoidal (divergence-free) vector fields', in J. Hinze (ed.) *Numerical Integration of Differential Equations and Large Linear Systems*, Springer Lecture Notes in Math. 968, 1982, pp. 95–113.
3. G. Fix, 'Finite element methods for flow problems', *Proc. IMACS World Congress*, Montreal, 1982, Vol. 1, pp. 28–29.
4. P. Gresho, R. Lee and R. Sani, 'On the time-dependent solution of the incompressible Navier–Stokes equations in two and three dimensions', *Recent Advances in Numerical Methods in Fluids*, Pineridge Press, Swansea, U.K., 1980, pp. 27–79.
5. R. Sani, P. Gresho, R. Lee, D. Griffiths and M. Engleman, 'The cause and cure (?) of the spurious pressures generated by certain FEM solutions of the incompressible Navier–Stokes equations', *Int. J. Num. Meth. Fluids*, **1**, 17–43 and 171–204 (1981).
6. M. Fortin, 'Old and new finite elements for incompressible flows', *Int. J. Num. Meth. Fluids*, **1**, 347–364 (1981).

7. K. Gustafson and R. Hartman, 'Divergence-free bases for finite element schemes in hydrodynamics', *SIAM J. Num. Anal*, **20**, 697–721 (1983).
8. J. L. Hess, 'Review of integral-equation techniques for solving potential-flow problems with emphasis on the surface-source method', *Computer Methods in Applied Mechanics and Engineering*, **5**, 145–196 (1975).
9. F. T. Johnson and P. E. Rubbert, 'Advanced panel-type influence coefficient methods applied to subsonic flow', *AIAA Paper 75-50* (1975).
10. T. A. Cruse and F. J. Rizzo (eds), *Boundary-Integral Equation Methods: Computational Applications in Applied Mechanics*, 'ASME applied mechanics symposia series', 11, AMD, 1975.
11. A. Mayo, 'The fast solution of Poisson's and the biharmonic equation on irregular regions', in R. Vichnevetsky and R. S. Stephens (eds), *Advances in Computer Methods for Partial Differential Equations—IV*, IMACS, 1981, pp. 107–111.
12. F. T. Johnson and R. M. James, personal communication.
13. W. Proskurowski and O. Widlund, 'On the numerical solution of Helmholtz's equation by the capacitance matrix method', *Math. Comp.*, **30**, 433–468 (1976).
14. D. P. O'Leary and O. Widlund, 'Capacitance matrix methods for the Helmholtz equation on general three-dimensional regions', *Math. Comp.*, **33**, 849–879 (1979).
15. W. Proskurowski and O. Widlund, 'A finite element-capacitance matrix method for the Neumann problem for Laplace's equation', *SIAM J. Sci. Stat. Comput.*, **1**, 410–425 (1980).
16. P. R. Garabedian, *Partial Differential Equations*, Wiley, New York, 1964.
17. K. E. Atkinson, *A Survey of Numerical Methods for the Solution of Friedholm Integral Equations of the Second Kind*, SIAM, Philadelphia, 1976.
18. A.S. L. Shieh, 'On the convergence of the conjugate gradient method for singular capacitance matrix equations for the Neumann problem of the Poisson equation', *Numer. Math.*, **29**, 307–327 (1978).
19. M. Dryja, 'A finite element-capacitance matrix method for the elliptic problem', *SIAM J. Numer. Anal.*, **20**, 671–680 (1983).
20. H. Krumhaar, 'Supersonic flutter of a circular cylindrical shell of finite length in an axisymmetrical mode', *Int. J. of Solids and Structures*, **1**, 23–57 (1965).
21. R. Richtmyer, 'Invariant manifolds and bifurcations in the Taylor problem', in K. Gustafson and W. Reinhardt (eds), *Quantum Mechanics in Mathematics, Chemistry, and Physics*, Plenum Press, New York, 1981, pp. 121–124.
22. R. W. Hockney and J. W. Eastwood, *Computer Simulation Using Particles*, McGraw-Hill, New York, 1981.
23. K. Gustafson, 'Hybrid fast Poisson solvers for fluid dynamics, transonic flow, solenoid projection and the Navier–Stokes equations for general domains', *IMACS Trans. on Scientific Computation*, **1**, 87–96 (1983). See also *Proc. IMACS World Congress*, 1982, Vol. 1, pp. 233–235.
24. G. Fairweather, F. J. Rizzo, D. J. Shippy and Y. S. Wu, 'On the numerical solution of two-dimensional potential problems by an improved boundary integral method', *J. Comp. Phys.*, **31**, 96–112 (1979).
25. D. P. Young, A. C. Woo, J. E. Bussoletti and F. T. Johnson, 'An exterior Poisson solver using fast direct methods and boundary integral equations with applications to nonlinear potential flow', *Boeing Commercial Airplane Company Technical Note D6-51792TN* (1982). To appear in *SIAM J. Sci. Stat. Comput.*
26. K. Halasi, 'Numerical solution of two dimensional potential problems using Fourier analysis, boundary integral equations, and near-far field concepts', *Doctoral dissertation*, University of Colorado at Boulder, 1983.
27. R. Peyret and T. D. Taylor, *Computational Methods for Fluid Flow*, Springer-Verlag, New York, 1983.
28. K. Gustafson and K. Halasi, 'On the divergence-free (i.e. mass conservation, solenoidal) condition in computational fluid dynamics: how important is it?', in C. Taylor, J. A. Johnson and W. R. Smith (eds), *Numerical Methods in Laminar and Turbulent Flow*, Pineridge Press, Swansea, U.K., 1983, pp. 617–626.
29. C. F. Carey and S. W. Kim, 'Lifting aerofoil calculation using the boundary element method', *Int. J. Num. Meth. Fluids*, **3**, 481–492 (1983).